Structure of Bimodal Polymer Brushes in a Good Solvent by Neutron Reflectivity

M. S. Kent*

Department 1815, Sandia National Laboratories, Albuquerque, New Mexico 87185

B. J. Factor,† Sushil Satija, and Pat Gallagher

National Institute of Standards and Technology, Gaithersburg, Maryland 20899

G. S. Smith

LANCSE, Los Alamos National Laboratories, Los Alamos, New Mexico 87545

Received October 4, 1995; Revised Manuscript Received January 22, 1996[⊗]

ABSTRACT: Neutron reflection is used to examine the concentration profile of bimodal tethered layers in a good solvent. The tethered layers are Langmuir monolayers of highly asymmetric poly(dimethylsiloxane)−polystyrene (PDMS−PS) diblock copolymers at the air surface of ethyl benzoate. The PS blocks dangle into the good solvent, while the PDMS blocks anchor the copolymers to the surface. Bimodal layers are prepared using two block copolymers which vary in the molecular weight of the dangling block. The presence of the smaller PS blocks (DOP = N_1) leads to additional stretching of the larger PS blocks (DOP = N_2) relative to their dimension in a single-component monolayer, while the dimension of the smaller PS blocks is largely unaffected by the presence of the larger blocks. For the three bimodal brushes examined, the effect of additional stretching for the larger chains is greatest (up to 30%) for $N_2 \cong 3N_1$, smaller for $N_2 \cong 5N_1$, and negligible for $N_2 \cong 11N_1$. These trends are in agreement with self-consistent field calculations reported in the literature. In addition, it is observed that the chains with shorter dangling blocks add preferentially to an existing copolymer monolayer when the chains in the monolayer are strongly interacting. This is attributed to a greater potential barrier for the longer chains to incorporate into the monolayer due to osmotic and steric interactions.

Introduction

Tethered chains, chains which are anchored by one end to a point or an interface, provide a convenient and powerful means of modifying interfacial properties.[1] Tethered chains have found application in such areas as lubrication, wetting, adhesion, and stabilization of colloidal dispersions, among others. Much experimental and theoretical work on single-component tethered layers has been reported in recent years.[1−4] However, under certain circumstances, it may not be possible to optimize desirable properties within the range of segmental profiles obtainable with single-component tethered layers. This motivates the study of the structure of mixed layers, for which a much larger range of segmental profiles are possible.

The properties of bimodal polymer brushes were first explored with analytical self-consistent field SCF treatments valid in the limit of strong stretching and for infinite molecular weight.[5,6] Several important results were obtained. First, it was shown that the ends for long and short chains segregate, such that the brush could be separated into inner and outer regions. This was subsequently demonstrated in Monte Carlo simulations.[7] In addition, the analytical SCF work showed that the longer chains are more highly stretched in the inner region of the brush than are the shorter chains. A third important conclusion from this work is that there is a thermodynamic advantage to mixing long and short chains due to the very low density of segments in the outer region of the brush. Dan and Tirrell[8] have examined bimodal brushes in greater detail by numerical SCF calculations. They reported segmental concentration profiles for the total brush and also separate profiles for the long and short chains. For the long chains, a maximum in the segment concentration appeared just beyond the inner region of the brush. This resulted from additional stretching of the long chains, and thus a depletion of long chain segments, in the inner region. They also examined the scaling of the thickness and the brush foot for both the inner and outer regions of the brush.

Previous experimental work on bimodal brushes involved measurements of the force profiles for bimodal brushes under compression.[9−11] Dhoot et al. studied bimodal brushes formed by adsorbing onto mica from solution either a binary distribution of polystyrene−poly(2-vinylpyridine) (PS−PVP) diblock copolymers or a PS−PVP−PS triblock copolymer in which the nonadsorbing PS blocks were of differing lengths.[11] These bimodal brushes were stable on the order of several days.[12] The force profiles for the bimodal brushes did not conform to the universal profile previously obtained for monodisperse diblock copolymers, a fact which is consistent with the presence of two characteristic length scales. However, the segmental profile is not obtained in the force measurement.

The experiments of Dhoot et al. provide an interesting contrast to an earlier study by Klein et al., which involved zwitterion-terminated PS chains adsorbing from solution onto mica.[9,10] Also using the surface forces apparatus, they reported that a bimodal distribution of chains in the brush was not stable when the concentrations of the two species in solution were comparable, but rather they observed a rapid (i.e., several hours) and complete replacement of long chains in a preformed brush by shorter chains. Ou-Yang and Gao using dynamic light scattering have also reported the replacement of longer chains by shorter chains in polymer brushes[13] but did not observe complete exchange as in

† Current address: Intel Corp., Chandler, AZ 85226.

[⊗] Abstract published in *Advance ACS Abstracts,* March 1, 1996.

0024-9297/96/2229-2843$12.00/0

Table 1. Description of Polymer Samples

copolymer sample	M_w (kg/mol) PDMS	PS	M_w/M_n	source
4−30	4	30	1.1	Polymer Labs (U.K.)
11−66	11	66	1.1	Polymer Standards Service (FRG)
20−170	21	169	1.06	Polymer Standards Service (FRG)
28−330	28	330	1.08	Polymer Standards Service (FRG)

the experiments of Klein et al. Their system involved end-functionalized poly(ethylene oxide) chains adsorbing onto colloidal silica particles. The differences in behavior in these three studies may be related to differences in anchoring energies, which may affect not only the equilibrium structure of the brush but also the ability of the brush to achieve equilibrium with chains in the reservoir on experimental time scales.

In this paper, we present the first direct measurements of the structure of bimodal tethered chain layers using neutron reflectivity. The model tethered chain systems which we employ are Langmuir monolayers of highly asymmetric poly(dimethylsiloxane)−polystyrene (PDMS−PS) diblock copolymers on the surface of ethyl benzoate (EB). For this system, the smaller PDMS blocks anchor the copolymers to the surface due to the low surface energy of PDMS, while the much larger PS blocks dangle into the good solvent. Since the neutron scattering length density of PDMS is nearly matched with air, only the fully deuterated submerged PS blocks contribute to the reflectivity. Thus, the focus of this work is the segmental concentration profile of the dangling PS blocks and, in particular, the two characteristic dimensions of the bimodal profile. In previous work on single-component monolayers, we have shown that the size of the anchoring PDMS blocks has no effect on the layer height of the submerged blocks.[14,15]

The present copolymer monolayers are stable over a range of surface densities, which can be achieved by decreasing the surface area for a fixed number of copolymers in the monolayer or by successive additions of copolymers to the surface at fixed area. In previous work, we monitored the surface pressure and reflectivity for single-component monolayers for up to 3 days, with no indication of chain desorption. The stability of these monolayers is attributed to the very large anchoring energies (∼kT/DMS monomer) which result from the difference in surface energy of PDMS and EB. For even a relatively short PDMS block of 100 monomer units, this anchoring energy is on the order of the strength of a covalent bond, much larger than typical adsorption energies at solid/liquid interfaces. Thus, this system contrasts with those for which there is exchange between chains in the brush and the liquid reservoir, where the surface density and composition are fixed by equilibrium considerations.

Below we compare the dimensions of the PS blocks in bimodal monolayers with those reported previously for single-component monolayers. The bimodal tethered layers are formed using two copolymers which vary in the molecular weight of the dangling PS block. We examine mixtures for which the ratio of the molecular weights of the submerged blocks ranges from 3 to 11. In addition, we also describe some interesting features of the spreading behavior.

Experimental Section

Materials. Three highly asymmetric PDMS−PS diblock copolymers with perdeuterated PS blocks were studied. The characterization data for these samples obtained from the suppliers are given in Table 1. The sample code corresponds to the molecular weights (kg/mol) of the PDMS and PS blocks, respectively. GPC traces typically reveal a small amount (<5%) of PS−PDMS−PS triblock material. EB was purchased from Aldrich and vacuum distilled before use.

Procedures. The bimodal monolayers were spread from dilute, equimolar solutions of the two copolymers in chloroform, a common good solvent for PDMS and PS. The concentrations (mol/mL) of each copolymer in the 11−66/20−170, 11−66/28−330, and 4−30/28−330 solutions were 2.4×10^{-8}, 4.8×10^{-9}, and 9.6×10^{-9}, respectively. For each experiment, the spreading solution was introduced to the EB surface using a Hamilton microsyringe. The surface tension was monitored with the Wilhelmy plate technique, using strips of filter paper and a Nima microbalance. Further details about the stability of the copolymer monolayers and the spreading behavior of PDMS and PS homopolymers are described in previous articles.[14,15] Since the spreading efficiency is <100% for these monolayers,[14,15] the surface density was determined by integrating model profiles fit to the reflectivity rather than from the volume of spreading solution deposited on the surface.

Neutron reflectivity measurements were performed on the NG7 reflectometer at NIST. A fixed wavelength of 4.1 Å was used. The critical edge for total reflection was obtained and used to normalize the data. The background intensity was determined from the intensity scattered just off the specular angle. The reflectivity data were collected for 4−6 h periods. Initially, the reflectivity from the bare EB surface was measured and compared to the calculated Fresnel reflectivity. A small shift in q of 0.0004 $Å^{-1}$ was required to bring the critical edge in line with that calculated for pure EB. This is attributed to a small uncertainty in the absolute angle of incidence.

The procedure used to fit the reflectivity data involved approximating the model profiles by a series of 2 Å thick slabs of constant concentration and then calculating the reflectivity from the stack of layers using the Fresnel equations with a Debye−Waller factor to describe the effect of roughness at the air surface.[16] The resolution, $\Delta q/q$, where Δq is the standard deviation of a Gaussian function, was fixed at 0.024. This value was determined by fitting the reflectivity data for the pure solvent surface. Best-fit parameters were determined by the minimization of $\chi^2 = \Sigma((R_{expt} - R_{calcd})^2/\sigma_{std}^2))/(N_{pts} - N_{param})$ using the Marquardt algorithm.

Results

Figure 1 shows sample reflectivity data for 11−66/20−170, 11−66/28−330, and 4−30/28−330 bimodal monolayers. The reflectivity from the monolayer covered surface is divided by the calculated Fresnel reflectivity for an air/EB interface with 3.8 Å roughness. This roughness value was obtained from least-squares regression to the reflectivity for the bare EB surface. The two peaks in each curve indicate the presence of two characteristic length scales in the monolayers.

The curves through the data in Figure 1 are best fits obtained from least-squares regression using the following model profile:

$$\phi(z) = \phi_{o,1}[1 - (z/h_1)^2] + \phi_{o,2}[1 - (z/h_2)^2] \qquad z \le h_1 < h_2$$

$$\phi(z) = \phi_{o,2}[1 - (z/h_2)^2] \qquad h_1 < z \le h_2 \qquad (1)$$

The best-fit profiles are shown in Figure 2. The model profile in eq 1 is adequate to describe the main features of the reflectivity curves as is shown by the comparisons in Figure 1. The only aspects of the profile that are used in the present analysis are the two characteristic dimensions and the component surface densities (obtained from the integral of the profile). The model profile in eq 1 is the simplest functional form (fewest adjustable parameters) for which these large-scale

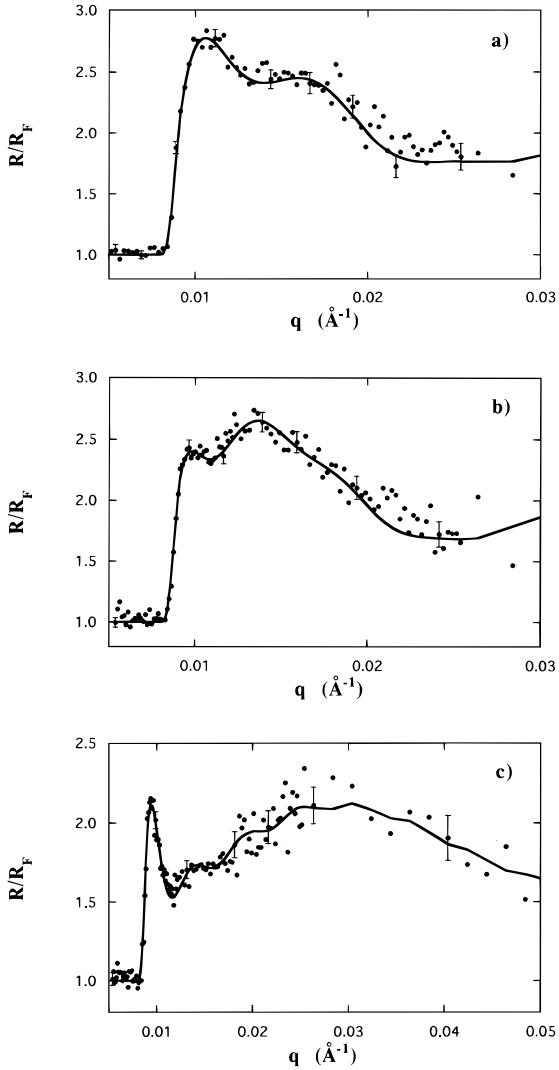

Figure 1. Reflectivity divided by the calculated reflectivity for a bare EB surface for the following bimodal monolayers: (a) 11−66/20−170, (b) 11−66/28−330, and (c) 4-30/28−330. The solid curves through the data are best fits calculated using the model profile in eq 1 of the text. The corresponding best-fit profiles are shown in Figure 2.

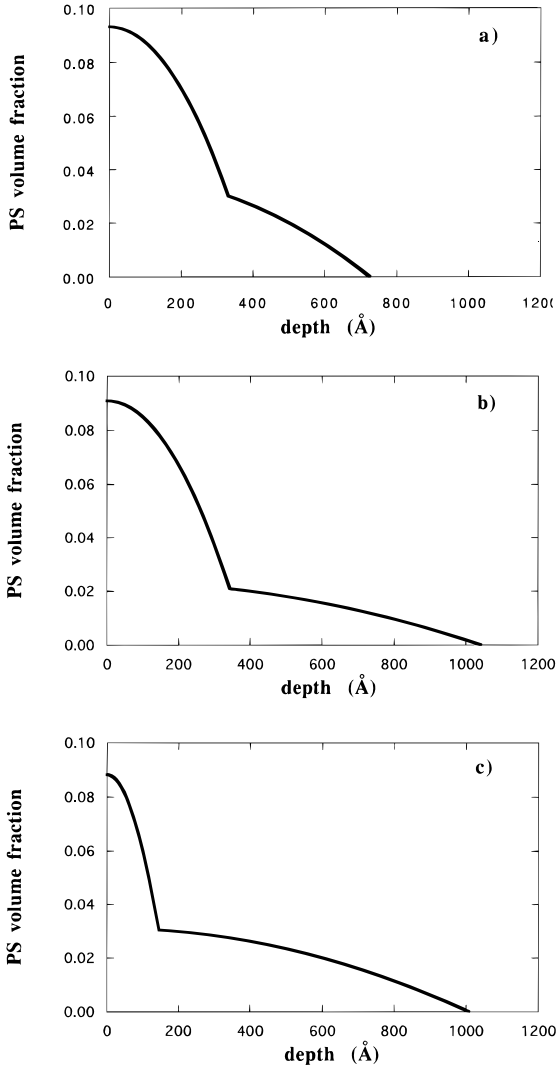

Figure 2. Best-fit profiles corresponding to the solid curves in Figure 1 for the following bimodal monolayers: (a) 11−66/20−170, (b) 11−66/28−330, and (c) 4−30/28−330.

features can be accurately extracted. No monomodal profile will describe the data from the mixed monolayers, as is clear from the presence of two peaks in each curve in Figure 1. The shape of the profile for each component in the bimodal monolayer lies between a step function and a linear function, as was observed for the single-component monolayers.[14,15] (The best fit using a sum of two linear functions or a sum of two step functions gives much larger χ^2 values and greater systematic deviations in the residuals than for eq 1.) There are, of course, a variety of functional forms which fall between a linear function and a step function, and a number of these (parabola, error function, shifted Gaussian, etc.) were compared previously for data from single-component monolayers.[15] It was shown that the best-fit χ^2 values are comparable for such profiles and that the maximum dimension and the integral of the profile are largely independent of the precise form used in the fitting.[15] The same is true for the present bimodal profiles. Equation 1 was selected from among these possible profiles because (i) it requires the fewest adjustable parameters among those that adequately describe the data and (ii) the characteristic dimensions are defined in a straightforward manner (h_1, h_2). Previous work on single-component monolayers has suggested the presence of a depletion layer near the surface and a smooth tail away from the surface.[15] These more detailed features are difficult to extract from a mixed monolayer and would require selective labeling of the individual components. These features will not be discussed in relation to the present data. We note that the profiles obtained from the reflectivity represent an average in the plane of the surface over the coherence area of the neutron beam ($\sim 1\ \mu m^2$). Thus, no information is obtained regarding the distribution of the copolymers in the plane of the surface.

Below we compare the characteristic dimensions in the mixtures with those in the single-component monolayers. However, such a comparison requires a knowledge of the surface density of each component in the mixed monolayer. To estimate these surface densities, we make the assumption that the profile in eq 1 can be resolved into two parabolas representing the contributions of the two components. This allows the surface density (σ_i) of each component to be estimated as:

$$\sigma_i = (\varrho N_A / M_{W,i}) \int_0^\infty \phi_i(z)\, dz \qquad (2)$$

where ρ and M_w are the melt density and molecular weight of the PS block, N_A is Avogadro's number, $\phi(z)$

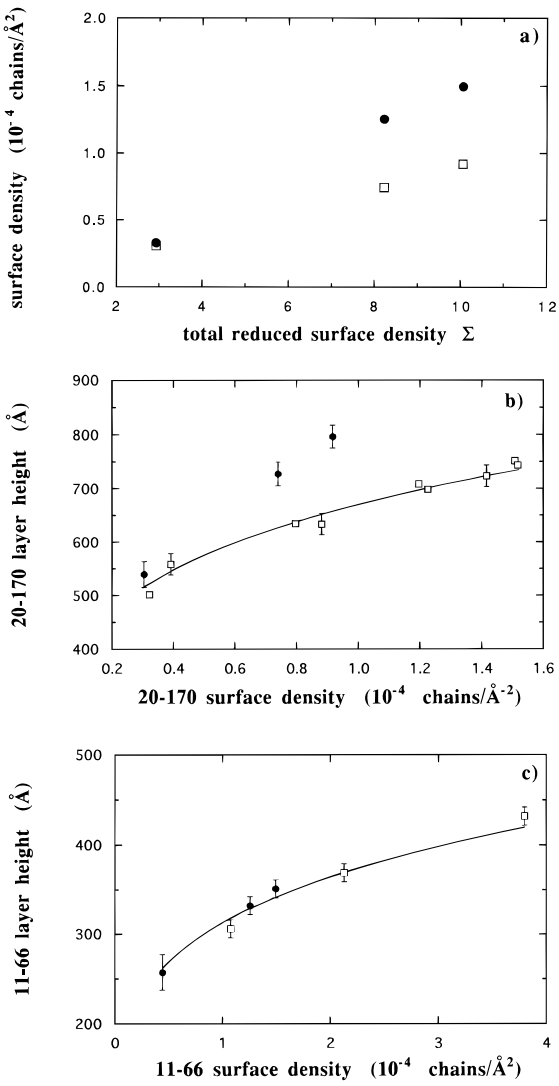

Figure 3. (a) Surface density of 11−66 (●) and 20−170 (□) copolymers versus the total reduced surface density for the 11−66/20−170 mixed monolayers. The surface pressures for the three monolayers were 0.4, 3.3, and 6.3 dyn/cm, increasing with increasing total surface density. (b) Comparison of the layer heights of the 170K PS blocks in the mixed monolayers (●) with those in the single-component 20−170 monolayers (□) as a function of 20−170 surface density. In the strongly interacting regime, the 170K blocks are more stretched in the bimodal monolayer than in the single-component monolayers. The curve through the single-component data corresponds to a power law dependence and is a guide to the eye.[17] (c) Comparison of the layer heights of the 66K PS blocks in the 11−66/20−170 mixed monolayers (●) with those in the single-component 11−66 monolayers (□) as a function of 11−66 surface density. In the strongly interacting regime, the 66K blocks have nearly the same dimension in the bimodal monolayer as in the single-component monolayers.

is the volume fraction of styrene (d8) segments, and z is the depth measured from the surface. Whereas an assumption is required to decompose the profile into component contributions and estimate the component surface densities, the two dimensions h_1 and h_2 are obtained directly from the experimental data (peak positions in Figure 1). The single-component data for the 4−30, 20−170, and 28−330 monolayers were reported previously.[15]

We begin with the data for the 11−66/20−170 mixed monolayers in Figure 3. The degree of interaction among the submerged blocks in the mixed monolayer can be inferred from the value of the total reduced surface density:

$$\sum = \sigma_{20-170}\,\pi R_{g,20-170}{}^2 + \sigma_{11-66}\,\pi R_{g,11-66}{}^2 \quad (3)$$

The condition $\Sigma = 1$ indicates when the submerged blocks begin to interact. In Figure 3a the surface density of each component is plotted versus the total reduced surface density for the three values of Σ examined. This plot shows the degree of interaction among the submerged blocks and the composition in each mixed monolayer. In these experiments, the surface density was increased from low to high values by successive addition of spreading solution to the surface. Figure 3a demonstrates that the composition of the monolayer was not constant as the total surface density of chains increased. Initially, the chains added to the surface in the same equimolar ratio as in the spreading solution. However, in subsequent additions the chains with the smaller submerged blocks added preferentially to the surface.

The effect of the 66K blocks on the dimension of the 170K blocks is shown in Figure 3b. In this figure, the layer heights for the 170K submerged blocks (h_{170}) in the 11−66/20−170 mixed monolayers are shown along with data obtained previously for the single-component 20−170 monolayer. The curve through the single-component data is a guide to the eye.[17] The surface density of the 20−170 copolymer is plotted on the abscissa for both the single-component and the mixed monolayers in order to allow a direct assessment of the affect of the 66K blocks on the dimension of the 170K blocks. The Σ value for each mixed monolayer is given in Figure 3a. At the lowest total surface density ($\Sigma \cong 3$), the value of h_{170} in the mixed monolayer is within experimental error of that obtained at the same surface density of 20−170 chains in the single-component monolayer. In this case, there is only weak interaction among the submerged blocks and the dimension of the 170K blocks is unaffected by the presence of the 66K blocks. However, at higher surface densities where the submerged blocks interact strongly, the layer heights for the 170K blocks are larger in the presence of the 11−66 copolymers than in their absence at the same σ_{20-170}. The additional stretching amounts to roughly 30% at the highest total surface density ($\Sigma \cong 10$).

Figure 3c compares the layer heights for the 66K PS blocks in the same mixed monolayers with data for the single-component 11−66 monolayers. In contrast to Figure 3b, little or no variation in the dimension of the shorter chains is observed due to the presence of the longer chains.

The analogous plots for the 11−66/28−330 mixed monolayers are shown in Figure 4. As for the 11−66/20−170 monolayers, it is observed in Figure 4a that for the initial deposition ($\Sigma \cong 4$) the composition in the monolayer is the same equimolar ratio as in the spreading solution. However, upon further addition of spreading solution to the surface, preferential addition of the smaller component again occurs. In this case the effect is much more pronounced than for the 11−66/20−170 mixture. In Figure 4b, the dimensions of the submerged 330K blocks in the mixed monolayers are compared with the dimensions in the single-component 28−330 monolayers. At the lowest reduced surface density, the dimension in the mixed monolayer is identical within experimental error with that in the absence of the 11−66 copolymer. At the higher surface density ($\Sigma \sim 9$),

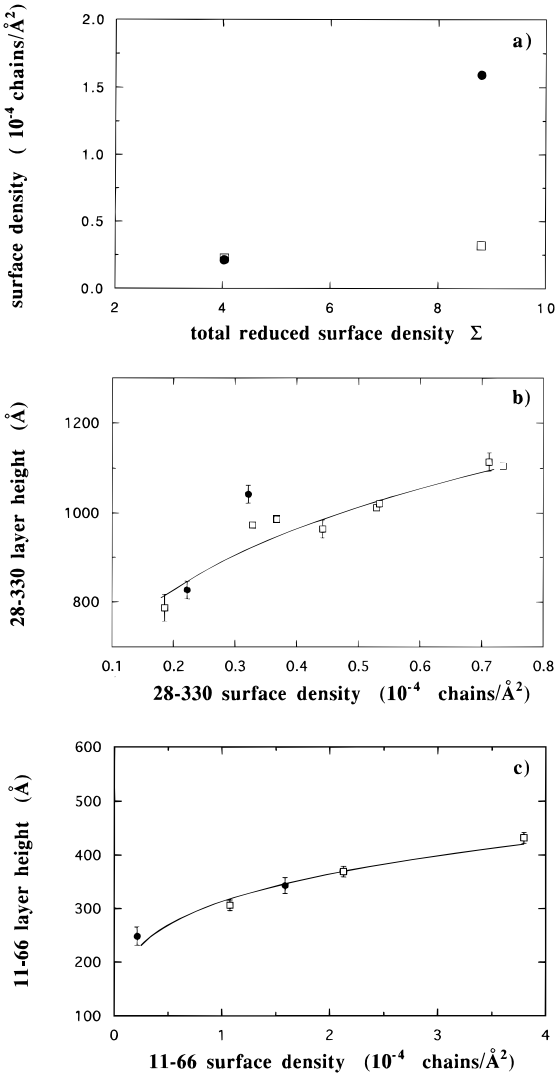

Figure 4. (a) Surface density of 11−66 (●) and 28−330 (□) copolymers versus the total reduced surface density for the 11−66/28−330 mixed monolayers. The surface pressures for the two monolayers were 0.5 and 5.2 dyn/cm, increasing with increasing total surface density. (b) Comparison of the layer heights of the 330K PS blocks in the mixed monolayers (●) with those in the single-component 28−330 monolayers (□) as a function of 28−330 surface density. In the strongly interacting regime, the 330K blocks are slightly more stretched in the bimodal monolayer than in the single-component monolayers. (c) Comparison of the layer heights of the 66K PS blocks in the 11−66/28−330 mixed monolayers (●) with those in the single-component 11−66 monolayers (□) as a function of 11−66 surface density. In the strongly interacting regime, the 66K blocks have nearly the same dimension in the bimodal monolayer as in the single-component monolayers.

where the submerged blocks interact strongly, the dimension of the longer blocks in the mixed monolayer is again observed to be larger relative to that in the absence of the shorter blocks. However, in this case, the effect (∼12%) is not nearly as large as for the 11−66/20−170 mixed monolayer, especially considering the much greater percentage of smaller chains in the monolayer.

Figure 4c compares the layer heights for the 66K PS blocks in the same mixed monolayers with data for the single-component 11−66 monolayers. As for the 11−66/20−170 mixtures, no variation in the dimension of the shorter chains is observed due to the presence of the longer chains.

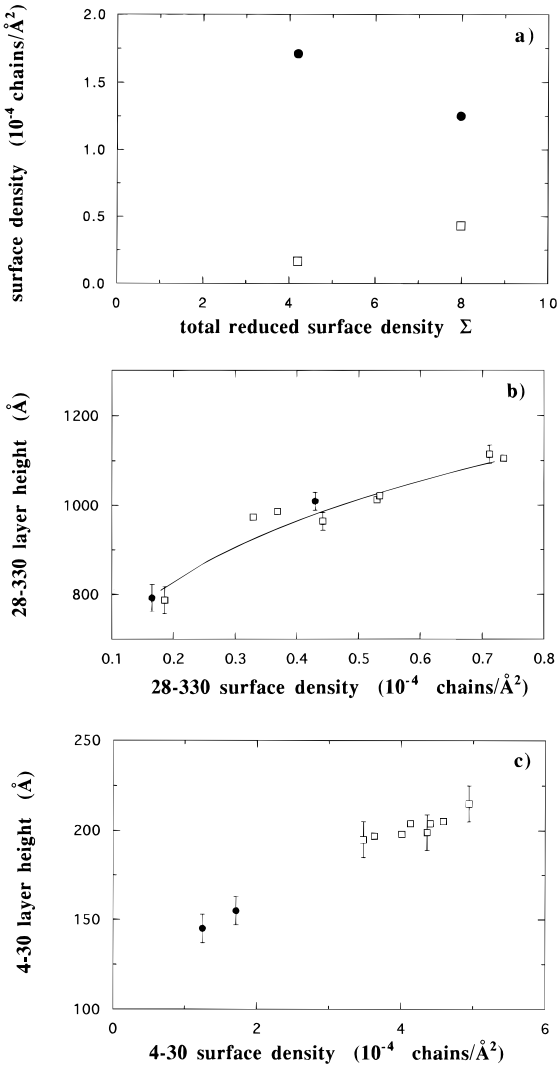

Figure 5. (a) Surface density of 4−30 (●) and 28−330 (□) copolymers versus the total reduced surface density for the 4−30/28−330 mixed monolayers. The surface pressures for the two monolayers were 0.6 and 2.1 dyn/cm, increasing with increasing total surface density. (b) Comparison of the layer heights of the 330K PS blocks in the mixed monolayers (●) with those in the single-component 28−330 monolayers (□) as a function of 28−330 surface density. In the strongly interacting regime, the 330K blocks have nearly the same dimension in the bimodal monolayer as in the single-component monolayers. (c) Comparison of the layer heights of the 30K PS blocks in the 4−30/28−330 mixed monolayers (●) with those in the single-component 4−30 monolayers (□) as a function of 4−30 surface density.

In Figure 5 the data for the third mixed monolayer, 4−30/28−330, are presented. In Figure 5a, once again the surface densities of each component are plotted versus Σ. In this case, the chains with the smaller submerged blocks are present in much higher percentage after the initial deposition (Σ ≅ 4). The 4−30 chains added preferentially to the surface in a ratio of ∼9/1 with the 28−330 chains. This result is consistent with the trend observed for the other mixed monolayers, although the preferential addition of the smaller component occurs at somewhat lower Σ values than for the other mixed monolayers. In moving to the higher surface density (Σ = 8), we observe surprisingly that the surface density of 4−30 chains is actually slightly lower than after the first addition. However, in this case, the surface was partially aspirated between the first and second additions to the surface. Thus, this

somewhat anomalous result is likely due to a preferential removal of the smaller chains during aspiration.

The layer heights of the submerged blocks for the 28−330 copolymer are compared with the dimensions in the single-component 28−330 monolayers in Figure 5b. For both surface densities we observe that the dimensions of the submerged 330K blocks in the mixed monolayers are identical within experimental error with those in the absence of the 4−30 copolymers. The analogous plot for the 4−30 copolymer is shown in Figure 5c. In this case, single-component data are not available for the entire range of surface density of the copolymer in the mixture. However, from an extrapolation of the available data, it appears that the dimension of the 4−30 copolymer in the presence of the 28−330 copolymer is comparable to that in the absence of the 28−330 copolymer.

Discussion

The results for the component dimensions in Figures 3−5 can be understood by considering the balance between the osmotic interaction of chain segments and entropically-based chain elasticity. For a single-component monolayer, the layer height is determined by a balance between the unfavorable osmotic interactions of the PS segments in the good solvent EB, which causes the chains to swell out from the surface, and the entropic penalty associated with distorting the chains from a random configuration. For the mixed monolayers, the stretching of each component chain will depend upon the variation of the total local segment concentration with depth from the surface. Consider first the 11−66/20−170 mixed monolayer at the highest total surface density, $\Sigma = 10$. In the mixed monolayer the presence of the 11−66 chains increases the segment concentration near the surface relative to that for the 20−170 single-component monolayer at the same σ_{20-170}. In the presence of the increased segment concentration gradient, the longer blocks swell further into the pure solvent subphase. The swelling of the longer chains induced by the shorter chains occurs only when the submerged blocks are strongly overlapping. No effect is observed for the lowest total reduced surface density ($\Sigma \cong 3$).

However, when the shorter chains in the same mixture are considered, it is observed that their dimension is nearly the same in the presence of the longer chains as in the absence of the longer chains. This is apparently due to the fact that the segments of the longer chains extend well beyond the dimension of the shorter chains. The presence of the 170K blocks increases the segment concentration throughout the extent of the 11−66 profile rather than just near the surface. Thus, the longer chains impose only a weak gradient in segment concentration on the shorter chains. There is therefore a much weaker driving force for the shorter chains to stretch away from the surface than for the longer chains. Comparing the effect observed for the three mixed monolayers, we find that the stretching of the larger chains induced by the shorter chains is greatest for $N_2 \cong 3N_1$, smaller for $N_2 \cong 5N_1$, and negligible for $N_2 \cong 11N_1$. This trend is as expected, since the perturbation of the profile of the longer chains due to the shorter chains must become negligible in the limit of $N_2 \gg N_1$. The trends in the results described above are consistent with the predictions of SCF calculations[8] and suggest that the longer chains are stretched in the inner region of the brush.

We note that if the longer chains are stretched in the inner region of the brush, there will be a depletion of long chain segments near the surface, and thus the segmental profile for the longer chains will deviate somewhat from a parabola. It then follows that the surface densities obtained above will not be precisely correct, since they were obtained by decomposing the total segmental profile into the sum of two parabolas. However, this uncertainty in the component profiles does not effect the conclusions of this work, since the assumption of parabolic component contributions will give an upper bound to the surface density of the longer chains. The amount of additional stretching of the longer chains inferred from the comparisons with the single-component data in Figures 3b and 4b will be even greater if the actual surfaces densities of the longer chains are lower than those obtained assuming parabolic profiles. The uncertainty in the decomposition into component profiles is illustrated in Figure 6, where the profile from Figure 2a is resolved into the component contributions based upon (i) pure parabolas (solid curves) and (ii) profiles qualitatively consistent with SCF calculations (dashed curves). For the longer chains, the surface density obtained from the parabolic profile is ∼20% larger than that obtained from the dashed profile. This is a reasonable estimate of this uncertainty. In future work we will attempt to obtain the component profiles directly by selectively deuterating only one of the two components.

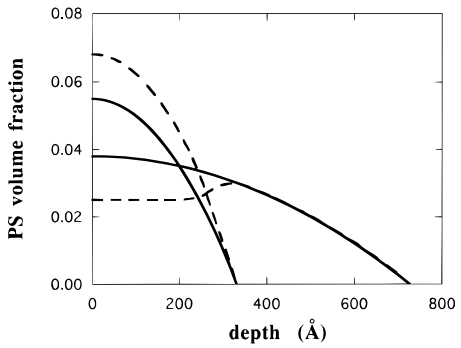

Figure 6. Illustration of the decomposition of the total bimodal segment density profile from Figure 2a into component profiles assuming (a) each component profile is purely parabolic (solid curves) or (b) the longer chain profile has a maximum just beyond the dimension of the shorter chains as predicted by SCF calculations (dashed curves).

The interesting observation that the chains do not always spread onto the surface in the same composition as in the spreading solution is believed to be a result of differing efficiencies for the two copolymers to incorporate into a monolayer of interacting chains. The general trends are as follows. When the chains are deposited onto a bare EB surface or a surface covered with a monolayer of chains which are noninteracting, they add to the monolayer in the same ratio as in the spreading solution. However, when the chains are deposited onto a surface which already contains a monolayer of interacting chains, the shorter chains add preferentially to the surface. This can be understood in terms of the relative sizes of the submerged blocks and the greater potential barrier for the longer chains to incorporate into the monolayer due to osmotic and steric interactions.[18]

The preferential addition of shorter chains to a polymer brush has also been reported in the studies involving competitive adsorption onto solid substrates[9,10,12] described in the Introduction. Among these studies, however, there are differences in the degree of preferential selection. Klein et al. observed a complete replacement of long chains by short chains when the

concentrations of the two species in solution were comparable. On the other hand, Dhoot et al., for similar solution conditions, observed stable bimodal distributions, albeit with a preferential adsorption of copolymers with smaller dangling blocks. As mentioned earlier, this difference may be due to differences in adsorption energies and/or the facility of exchange between the brush and the reservoir in each case. Klein et al. estimate the anchoring energy of the zwitterion on mica to be ~6−8 kT, while Dhoot et al. estimate the anchoring energies of their adsorbing PVP blocks on mica to range from ~15 to 32 kT. In both cases, the estimates are obtained using theoretical relations between adsorbed amounts and anchoring energies. In the case of Klein et al., the adsorption energy of the zwitterion is clearly low enough to allow chains in the brush to exchange rapidly with those in the reservoir, and therefore the system can achieve the lowest energy state. For $N_1 \ll N_2$ and for anchoring energies much greater than kT, Dan has shown that in the lowest energy state the brush is composed of only the shorter chains, when the concentrations of the two chains in the reservoir are comparable.[19] In the work of Dhoot et al., the length of the adsorbing blocks may lead to limited (or very slow) exchange due to higher adsorbing energies or topological effects inhibiting desorption. In that case the brush would be trapped in a state with only the partial selection of short chains which would have occurred during the initial construction of the brush. The fact that the anchoring energies are difficult to measure directly or vary over a wide range impedes a clear interpretation of the studies of competitive adsorption onto solid surfaces. Polymer brushes formed at the liquid/air interface can provide some insight in this regard, in that the anchoring energies are accessible experimentally from interfacial tension measurements[15] and can be varied systematically over a wide range by varying the subphase liquid. For the present system, the anchoring energies range from ~50 to ~350 kT, and there is virtually no exchange with chains in the reservoir.[15] (The concentration of chains in the reservoir is never greater than $\sim 10^{-7}$.) Therefore the present work demonstrates that free exchange with the bulk is not required for preferential addition of shorter chains to occur but that such an effect can result from interactions during the initial construction of the brush.

In the present work, the fact that the composition in the monolayer varies as the total surface density increases complicates a quantitative comparison with theoretical predictions. However, it does not affect the principal qualitative result, that the presence of the shorter chains leads to stretching of the longer chains, while the presence of the longer chains has little influence on the dimension of the shorter chains.

Conclusions

An experimental study of the structure of bimodal polymer brushes in good solvents is presented based upon neutron reflectivity from Langmuir diblock copolymer monolayers. At high surface densities where the chains are strongly interacting, the presence of the shorter chains leads to additional stretching of the longer chains, presumably in the inner region of the brush, whereas the dimension of the shorter chains is relatively unaffected by the presence of the longer chains. The magnitude of the effect is ~30% for $N_2 \cong 3N_1$ and decreases as the difference in chain length increases. These trends are in qualitative agreement with SCF calculations. Preferential addition to an existing monolayer of chains with shorter dangling blocks is observed when the chains in the monolayer are strongly interacting. This is attributed to a greater potential barrier for the longer chains to incorporate into the monolayer due to osmotic and steric interactions.

Acknowledgment. This work was partially supported by the U.S. Department of Energy under contracts DE-AC04-94AL85000 and W-7405-ENG-36. We gratefully acknowledge helpful discussions with N. Dan.

References and Notes

(1) Halperin, A.; Tirrell, M.; Lodge, T. P. *Adv. Polym. Sci.* **1992**, *100*, 31.
(2) Patel, S.; Tirrell, M. *Annu. Rev. Phys. Chem.* **1989**, *40*, 597.
(3) Grest, G. S.; Murat, M. Computer Simulations of Tethered Chains. In *Monte Carlo and Molecular Dynamics Simulations in Polymer Science*; Binder, K., Ed.; Clarendon Press: Oxford, 1994.
(4) Szleifer, I. *Adv. Chem. Phys.* **1996**, *94*, Chapter 3.
(5) Milner, S. T.; Witten, T. A.; Cates, M. *Macromolecules* **1989**, *22*, 853.
(6) Birshtein, T. M.; Liatskaya, Y. V.; Zhulina, E. B. *Polymer* **1990**, *31*, 2185.
(7) Chakrabarti, A.; Toral, R. *Macromolecules* **1990**, *23*, 2016.
(8) Dan, N.; Tirrell, M. *Macromolecules* **1993**, *26*, 6467.
(9) Klein, J.; Kamiyama, Y.; Yoshizawa, H.; Israelachvili, J. N.; Fetters, L. J.; Pincus, P. *Macromolecules* **1992**, *25*, 2062.
(10) Kumacheva, E.; Klein, J.; Pincus, P.; Fetters, L. J. *Macromolecules* **1993**, *26*, 6477.
(11) Dhoot, S.; Watanabe, H.; Tirrell, M. *Colloids Surf.* **1994**, *86*, 47.
(12) Dhoot, S.; Tirrell, M. *Macromolecules* **1995**, *28*, 3692.
(13) Gao, Z.; Ou-Yang, H. D. *ACS Symp. Ser.* **1993**, *532*, 70.
(14) Kent, M. S.; Lee, L. T.; Farnoux, B.; Rondelez, F. *Macromolecules* **1992**, *25*, 6240.
(15) Kent, M. S.; Lee, L. T.; Factor, B. J.; Rondelez, F.; Smith, G. S. *J. Chem. Phys.* **1995**, *103* (6), 2320.
(16) Russell, T. P. *Mater. Sci. Rep.* **1990**, *5*, 171.
(17) In our previous work we demonstrated that single-component data for six samples ranging in molecular weight from 30K to 330K can be represented by either a linear dependence of h/R_g on Σ or a power law relation of the form $h \sim M^{\alpha}\sigma^{\beta}$. The lines drawn through the single-component data in Figures 3−5 correspond to power law dependencies, although none of the conclusions of this work are altered if the linear representation for the single-component data is chosen.
(18) Milner, S. T. *Macromolecules* **1992**, *25*, 5487.
(19) Dan, N. *Macromolecules* **1994**, *27*, 2310.

MA951497D